Microwave Photonic Interrogation of a High-Speed and High-Resolution Temperature Sensor Based on Cascaded Fiber-Optic Sagnac Loops

Guangying Wang, Baoliang Liao, Yuan Cao, Xinhuan Feng, Bai Ou Guan, *Fellow, OSA*, and Jianping Yao, *Fellow, OSA*

***Abstract*—A high-speed and high-resolution temperature sensor based on two cascaded fiber-optic Sagnac loops (FSLs) interrogated using a microwave photonic (MWP) method is proposed and experimentally demonstrated. In the proposed system, an FSL is used as a sensor element. When it is experiencing temperate change, its spectrum is shifted, which leads to the shift in the spectrum of the cascaded FSLs. Instead of measuring the wavelength shift of the spectrum by using an optical spectrum analyzer (OSA), which has a low wavelength resolution and a slow scanning speed, we convert the optical spectrum to the time domain based on spectral shaping and wavelength-to-time (SS-WTT) mapping, and use a digital signal processor (DSP) to extract the sensing information. In our experiment, two cascaded FSLs with two different free spectrum ranges (FSRs) are employed. Due to the Vernier effect, multiple dips in the envelope of the optical spectrum are introduced. By passing a broadband frequency-chirped optical pulse generated by a frequency-swept laser source to the two cascaded FSLs, the sensing information is encoded in the optical spectrum and it is converted to the time domain due to SS-WTT mapping. By detecting the optical waveform at a photodetector (PD), a temporal microwave waveform with its shape identical to the optical spectrum is generated. By using a DSP, the time shift of a dip is measured and the sensing information is precisely demodulated. Experimental result shows that the proposed fiber-optic temperature sensor can provide a temperature resolution of 1.33 $\times$ 10^{-5} °C at a sensing speed of 23.497 kHz.**

***Index Terms*—Cascaded fiber-optic Sagnac loops, fiber-optic sensor, microwave photonics, temperature measurement, Vernier effect.**

Manuscript received June 8, 2020; revised September 11, 2020 and October 26, 2020; accepted October 28, 2020. Date of publication November 2, 2020; date of current version June 16, 2021. This work was supported by National Natural Science Foundation of China (NSFC) under Grant 61860206002, Grant 61701193, and Grant 61771221. *(Corresponding authors: Yuan Cao; Xinhuan Feng.)*

Guangying Wang, Baoliang Liao, Yuan Cao, Xinhuan Feng, and Bai Ou Guan are with the Guangdong Province Key Laboratory of Optical Fiber Sensing and Communications, Institute of Photonics Technology, Jinan University, Guangzhou 510632, China (e-mail: guangyingwang@stu2017 jnu.edu.cn; baoliang@stu2019.jnu.edu.cn; caoyuan@jnu.edu.cn; eexhfeng@gmail.com; tguanbo@jnu.edu.cn).

Jianping Yao is with the Guangdong Province Key Laboratory of Optical Fiber Sensing and Communications, Institute of Photonics Technology, Jinan University, Guangzhou 510632, China, and also with the Microwave Photonics Research Laboratory, School of Electrical Engineering and Computer Science, University of Ottawa, Ottawa, ON K1N 6N5, Canada (e-mail: jpyao@jnu.edu.cn).

Color versions of one or more of the figures in this article are available online at https://ieeexplore.ieee.org.

Digital Object Identifier 10.1109/JLT.2020.3035259

I. Introduction

ACCURATE measurements and control of temperature based on optical fiber sensors could find numerous applications such as environmental monitoring, medical diagnostics, and chemical reaction control [1]. For the past few decades, optical fiber sensors have been intensively studied due to their intrinsic advantages such as compact size, immunity to electromagnetic interference, high sensitivity, low cost, high resistance to erosion and remote sensing ability [2]. Recently, several configurations of fiber-optic temperature sensors based on fiber gratings have been proposed and experimentally demonstrated. The fiber gratings include fiber Bragg gratings (FBGs) [3], long period fiber gratings (LPFGs) [4], and tilted fiber Bragg gratings (TFBGs) [5]. However, grating-based optical fiber temperature sensors usually have a relatively low sensitivity of 10∼100 pm/°C. To enhance the sensitivity, numerous other optical fiber sensors such as photonic crystal fiber-based sensors [6], [7] and tapered optical microstructure fiber-based sensors [8] have been proposed and experimentally demonstrated. Recently, the Vernier effect which is proved to be an effective way to enhance the sensitivity of an optical fiber sensor, has been adopted to improve the performance for temperature, gas refractive index and ammonia concentrations measurements [9]–[12] by using a structure such as cascaded FSLs [9], cascaded Fabry-Perot interferometers (FPIs) [10] and cascaded Mach-Zehnder interferometers (MZIs) [11]. Normally, the optical spectrum of a single MZI, FPI or FSL has a fixed free spectrum range (FSR) and a flat spectrum envelop. By cascading a second MZI, FPI or FSL with a slightly different FSR, due to the Vernier effect, the envelope of the spectrum will have multiple dips. When the MZI, FPI or FSL is experiencing an environmental change, the envelope of the spectrum will shift accordingly. Through measuring the wavelength shift by locating a dip in the envelope by using an optical spectrum analyzer (OSA), the sensing information is demodulated with a greatly enhanced sensitivity. However, to precisely measure the location of a dip in the envelope is extremely difficult since an OSA-based wavelength demodulation method usually has a very low wavelength resolution. In addition, the slow scanning speed of an OSA makes it difficult to detect a fast change temperature.

Microwave Photonics (MWP) [13], [14], a technique to generate and process microwave signals directly in the optical domain,

0733-8724 © 2020 IEEE. Personal use is permitted, but republication/redistribution requires IEEE permission.
See https://www.ieee.org/publications/rights/index.html for more information.

Authorized licensed use limited to: Jianping Yao. Downloaded on December 16,2021 at 03:23:19 UTC from IEEE Xplore. Restrictions apply.

has been widely studied recently and it is considered an effective way to realize high-speed and high-resolution sensing demodulation. Recently, high-speed and high-resolution temperature and strain sensors based on microwave photonic interrogation have been proposed and experimentally demonstrated [15], [16]. Instead of monitoring the wavelength shift of an optical spectrum, the optical spectrum is converted to the time domain based on spectral shaping and wavelength-to-time (SS-WTT) mapping. Thus, the sensing information can be demodulated in the electrical domain using a digital signal processor (DSP) with an increased measurement speed and resolution.

In this paper, we propose and experimentally demonstrate a high-speed and high-resolution temperature sensor based on two cascaded FSLs interrogated based on a microwave photonics method. Instead of monitoring the wavelength shift of the optical spectrum by using an OSA, which has a poor wavelength resolution and a low scanning speed, we convert the optical spectrum to a microwave waveform in the time domain based on SS-WTT mapping, and demodulate the sensing information using a DSP at a high speed and high resolution. In the proposed temperature sensing system, by passing a broadband chirped optical pulse generated by a high-speed frequency-swept laser source to the two cascaded FSLs, the sensing information is encoded in the spectrum and the spectrum is mapped to the time domain. The two FSLs have different FSRs, due to the Vernier effect, the envelope of the optical spectrum will have multiple dips. When a temperature change is applied to one of the FSLs, the envelope of the optical spectrum will shift which is also reflected in the time-domain waveform. By detecting the time-domain waveform at a photodetector (PD), a temporal microwave waveform with its shape identical to the shaped spectrum is generated. A DSP is then used to extract the envelope in the time domain at a high speed and high resolution. By monitoring the time shift of a dip in the envelope, the sensing information is demodulated. The proposed approach is evaluated experimentally. The experimental result shows the proposed temperature sensor can provide a temperature resolution of 1.33 $\times 10^{-5}$ °C at a high sensing speed of 23.497 kHz.

II. Principle and Experimental Setup

For an FSL with a polarization-maintaining-fiber (PMF) loop having a length of L and a birefringence of B, its transmission spectrum can be mathematically expressed by

$$T(\lambda) = \frac{1+\cos(\varphi)}{2} \tag{1}$$

where $\varphi = 2\pi BL/\lambda$, and λ is the optical wavelength.

The FSR of a single FSL is given by

$$FSR_{FSL} = \frac{\lambda^2}{BL} \tag{2}$$

Fig. 1(a) and (b) shows the simulated transmission spectra of two FSLs with two different FSRs. When the loop lengths of the first and the second FSLs are 1.71 and 1.90 m and the birefringence of the PMF is 5.85×10^{-4}, the FSRs are calculated to be 2.4 nm and 2.16 nm, respectively.

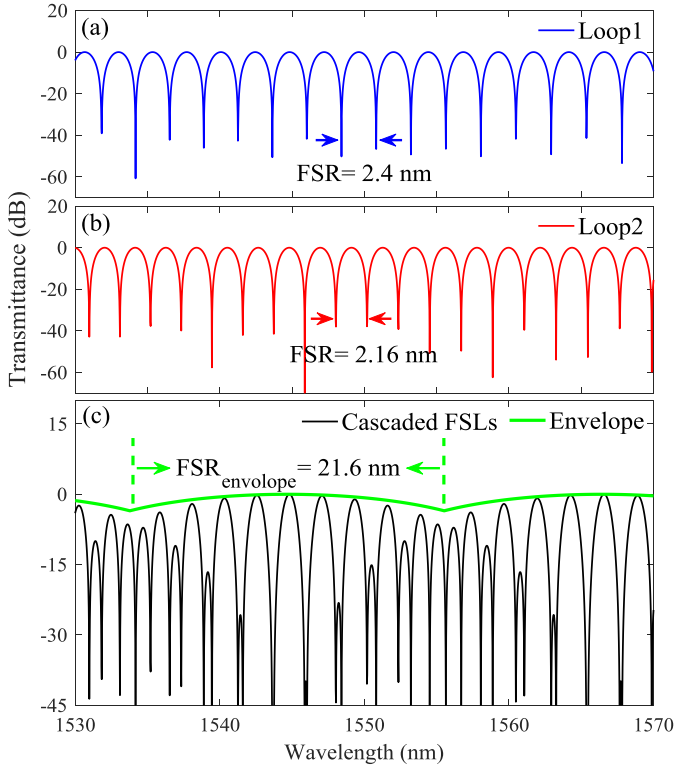

Fig. 1. Simulated transmission spectra of the two FSLs with an FSR of (a) 2.4 nm and (b) 2.16 nm; (c) Black: simulated transmission spectrum of the two cascaded FSLs; Green: envelope introduced by the Vernier effect.

The transmission spectrum of the two cascaded FSLs can be expressed by

$$T'(\lambda) = \left[\frac{1+\cos\left(\frac{2\pi BL_1}{\lambda}\right)}{2}\right]\left[\frac{1+\cos\left(\frac{2\pi BL_2}{\lambda}\right)}{2}\right] \tag{3}$$

where L_1 and L_2 are the lengths of the PMFs in the first and the second FSL, respectively.

Fig. 1(c) shows overall transmission spectrum of the two cascaded FSLs. The green curve shows the envelope. As can be seen, by cascading the two FSLs, due to the Vernier effect, the power distribution of the optical spectrum is no longer flat, but has an envelope with multiple dips. The distance between two adjacent dips is the total FSR of the two cascaded FSLs, which is given by

$$FSR_{envelope} = \frac{FSR_1 \cdot FSR_2}{|FSR_1 - FSR_2|} \tag{4}$$

where FSR_1 and FSR_2 are the FSRs of the first and the second FSLs, respectively. As can be seen from Fig. 1(c), the FSR is significantly increased.

Once the temperature applied to the sensing loop is increased, the birefringence of the PMF in the sensing loop will decrease and the transmission spectrum of the sensing loop will shift to a smaller wavelength. Therefore, the envelope in the transmission spectrum of the two cascaded FSLs will shift to a longer wavelength. Fig. 2(a) shows the simulated transmission spectra of

Authorized licensed use limited to: Jianping Yao. Downloaded on December 16,2021 at 03:23:19 UTC from IEEE Xplore. Restrictions apply.

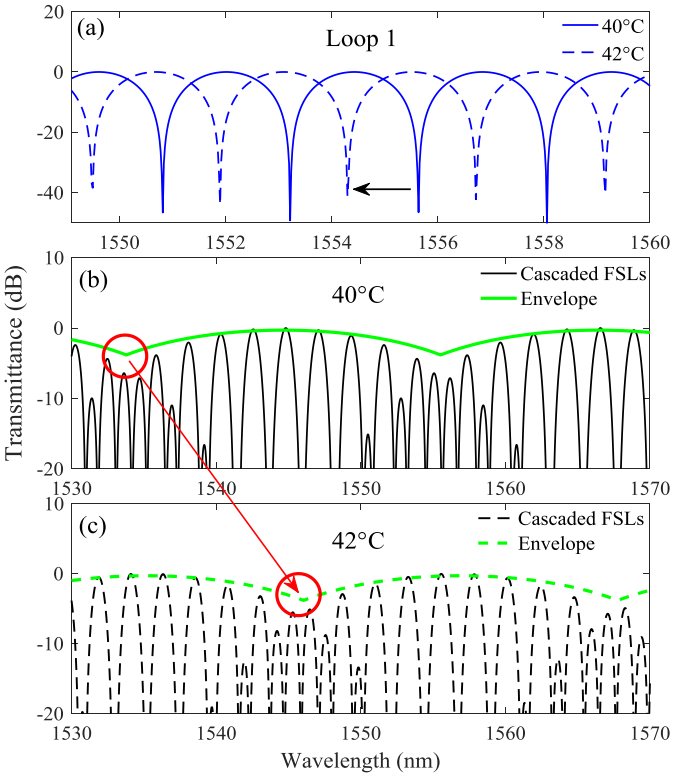

Fig. 2. (a) Spectrum shift when the temperature applied to the sensing loop is increased from 40 to 42 °C; (b) The simulated transmission spectrum of the two cascaded FSLs (black) and the introduced envelope (green) when the temperature of the sensing loop is 40 °C; (c) The simulated transmission spectrum of the two cascaded FSLs (black dash) and the introduced envelope (green dash) when the temperature of the sensing loop is 42 °C. The dip in (b) is shifted to a longer wavelength.

the sensing loop when the temperature applied to the loop is increased from 40 to 42 °C. From the simulated results we can see that, as the temperature applied to the sensing loop is increased, the transmission spectrum will shift to a smaller wavelength. Fig. 2(b) and (c) shows the simulated transmission spectra of the two cascaded FSLs before and after the temperature change. We can see that, as the applied temperature is increased, the envelope of the spectrum is shifted to a longer wavelength, and the wavelength shift of the envelope can be calculated by

$$\Delta\lambda_{envelope} = \lambda\left(\frac{\Delta B\,(T)}{B}\right)\left(\frac{FSR_2}{|FSR_2 - FSR_1|}\right) \tag{5}$$

where $\triangle B(T)$ is the birefringence change of the PMF incorporated in the sensing loop, which is a function of the temperature change. Thus, the sensitivity enhanced factor of the two cascaded Sagnac loops can be expressed by

$$M = \frac{FSR_2}{|FSR_2 - FSR_1|} \tag{6}$$

Actually, we can consider that when the temperature applied to the sensing loop is increased, a change in the envelope in the optical domain is resulted, which leads to the change in the envelope of the time-domain microwave waveform obtained after wavelength-to-time mapping. By extracting the envelope in the time domain and detecting the location of a dip, the sensing information is demodulated.

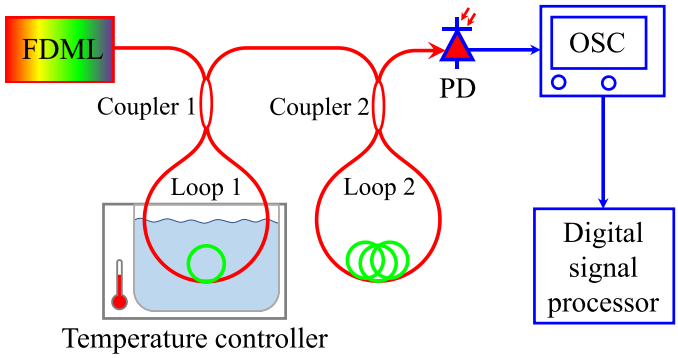

Fig. 3. Schematic diagram of the proposed temperature sensor based on two cascaded FSLs interrogated based on microwave photonic method.

The schematic diagram of the proposed high-speed and high-resolution temperature sensor based on two cascaded FSLs is shown in Fig. 3. It consists of a frequency-swept laser source which is a Fourier domain mode-locked (FDML) laser source [17], two cascaded FSLs and a PD. The FDML laser source is used to provide a broadband frequency-chirped optical pulse train which is applied to the two cascaded FSLs with the first FSL placed in a temperature controller as a sensing element.

It should be noted that, instead of using a dispersive element to achieve wavelength-to-time mapping [18], the optical pulse from the FDML laser source is chirped. Passing a frequency-chirped optical pulse through the cascaded FSLs will perform sensing information encoding and, at the same time, wavelength-to-time mapping [19]. The Fourier domain mode locking of the FDML laser source is performed using a sinusoidal signal to achieve the frequency tuning of a tunable optical filter in the FDML laser cavity. Mathematically, the instantaneous wavelength of the frequency-chirped optical pulse at the output of the FDML laser can be expressed by

$$\lambda\,(t) = \lambda_0 + \frac{1}{2}\Delta\lambda\,[1 - \sin\,(2\pi f t)] \tag{7}$$

where λ_0, $\triangle\lambda$ and f are the starting wavelength, wavelength scanning bandwidth, and the repetition rate of the pulse train of the FDML laser, respectively.

When an optical pulse is applied to the two cascaded FSLs, the spectrum of the optical pulse is spectrally shaped and the sensing information is encoded in the spectrum. Note that since the optical pulse entering the cascaded FSLs is frequency chirped, the spectrum is shaped and mapped to the time domain [20]. The spectrally shaped time-domain optical pulse is then launched to a PD, a temporal microwave waveform is generated. A real-time oscilloscope connected to the PD is employed to sample the time-domain microwave signal and a DSP is used to process the sampled signal.

Since the optical pulse generated by the FDML laser source has a nonlinear relationship between the wavelength and time (due to the use of a sinusoidal function as a mode locking

Authorized licensed use limited to: Jianping Yao. Downloaded on December 16,2021 at 03:23:19 UTC from IEEE Xplore. Restrictions apply.

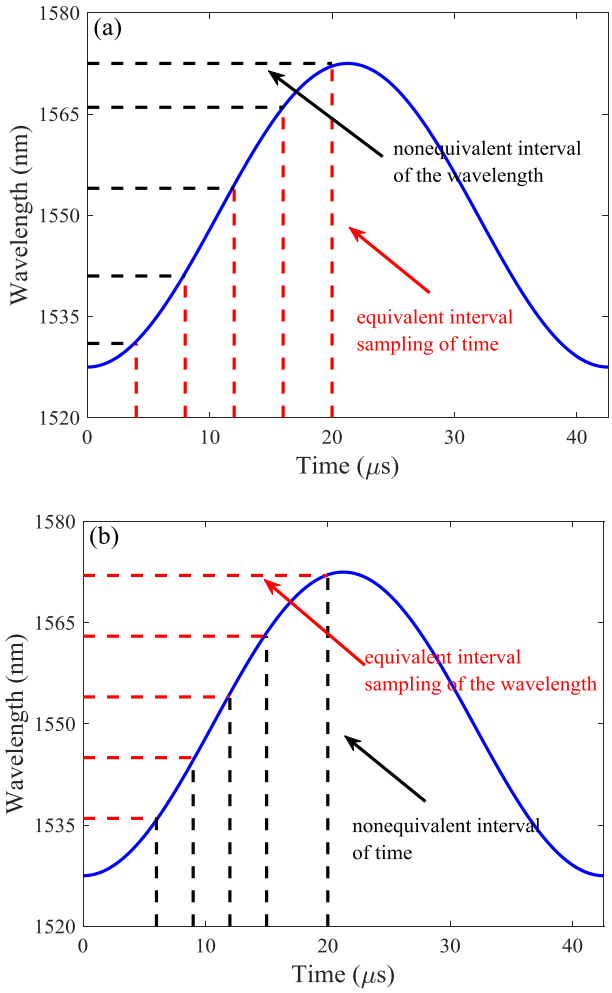

Fig. 4. Nonlinear to linear wavelength-to-time mapping conversion via resampling. (a) Nonlinear wavelength-to-time relationship of a microwave waveform sampled with an identical interval; (b) Resampling with a nonidentical sampling interval to make the nonlinearly wavelength-to-time mapping linear.

signal), the transmission spectrum of the two cascaded FSLs is nonlinearly mapped to the time domain, which is given by

$$y(t) = \left\{\frac{1+\cos\left[\frac{2\pi BL_1}{\lambda(t)}\right]}{2}\right\}\left\{\frac{1+\cos\left[\frac{2\pi BL_2}{\lambda(t)}\right]}{2}\right\} \tag{8}$$

The nonlinear wavelength-to-time mapping should be corrected. Fig. 4(a) shows the nonlinear wavelength-to-time mapping relationship due to the use of a sinusoidal function as a mode locking signal. As can be seen if a wavelength-to-time mapped microwave waveform is sampled by an oscilloscope with an identical sampling interval, the optical spectrum will be nonlinearly mapped to the time domain. To make the nonlinear wavelength-to-time mapping relationship linear, a simple solution is to use a resampling process which can be implemented in the DSP. As shown in Fig. 4(b), by resampling the microwave waveform with a nonidentical time interval, the nonlinear (sinusoidal) wavelength-to-time mapping relationship is converted to

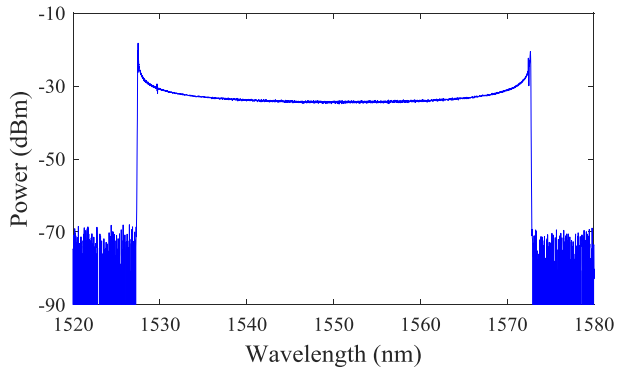

Fig. 5. The optical spectrum of the FDML laser source.

linear. The time interval employed in the resampling process is calculated based on (6), which is given by

$$t = \frac{\arcsin\left[1+\frac{2(\lambda_0-\lambda')}{\Delta\lambda}\right]}{2\pi f} \tag{9}$$

where λ' is the discrete values of the wavelengths corresponding to the sampling with an identical interval shown in Fig. 4(a). After the resampling operation, the wavelength-to-time mapping becomes linear.

We would like to emphasize that the purpose of the resampling process is to convert the nonlinear (sinusoidal) relationship between the instantaneous wavelength and time to a linear relationship. After the conversion, the wavelength-to-time mapping relationship becomes linear and the transmission spectrum at the output of the two cascaded FSLs is linearly mapped to the time domain, which is mathematically expressed by

$$y'(t) = \left[\frac{1+\cos\left(\frac{2\pi BL_1}{\lambda_0+kt}\right)}{2}\right]\left[\frac{1+\cos\left(\frac{2\pi BL_2}{\lambda_0+kt}\right)}{2}\right] \tag{10}$$

where $k = 2\triangle\lambda f$ is the wavelength scanning rate of the new linear wavelength-to-time relationship of the FDML laser source.

Then, a dip in the envelope introduced due to the Vernier effect is detected and its location is representing the wavelength shift of the optical spectrum. By monitoring the time shift of the dip, the sensing information is demodulated at a high-speed and high-resolution.

III. Experimental Results

An experiment based on the schematic diagram shown in Fig. 3 is implemented. A high-speed and broadband frequency-chirped optical pulse train with a repetition rate of 23.497 kHz, a spectrum width of 45 nm, and a central wavelength of 1550 nm generated by an FDML laser source is applied to the two cascaded FSLs. Fig. 5 shows the optical spectrum of the FDML laser source.

The lengths of the PMFs incorporated in the first and the second FSLs are 1.28 m and 1.37 m long, respectively. The FSL with a 1.28 m long PMF incorporated in the first FSL is placed in

Authorized licensed use limited to: Jianping Yao. Downloaded on December 16,2021 at 03:23:19 UTC from IEEE Xplore. Restrictions apply.

a temperature controller as a sensing element. The birefringence of the PMFs is 5.85×10^{-4} and the FSRs of the two FSLs are calculated to be 3.2 nm and 3.0 nm, respectively, according to (2). The total FSR of the two cascaded FSLs is calculated to be 48 nm according to (4). By applying a broadband optical pulse train generated by the FDML laser source to the two cascaded FSLs, the spectrum of the optical pulse is spectrally shaped and is mapped to the time domain, where the sensing information is encoded. The SS-WTT mapped optical pulse is then launched to a PD (Thorlabs, PDB570C), where a time domain microwave waveform is generated. At the output of the PD, a real-time oscilloscope (Tektronix, DSA72004B) which is synchronized by the FDML laser source is employed to sample the temporal microwave waveform. The sampled temporal microwave waveform is processed in a DSP to extract the envelope of the time-domain microwave signal.

Fig. 6(a) shows a temporal microwave waveform sampled by the real-time oscilloscope after spectrally shaped by the two cascaded FSLs. As can be seen, the transmission spectrum of the two cascaded FSLs is nonlinearly mapped from the optical domain to the time domain since the instantaneous output wavelength versus time is a sinusoidal function. Then, the waveform is sent to a DSP, at which a resampling process is performed and the sensing information encoded in the microwave waveform is demodulated. The blue curve in Fig. 6(b) shows a resampled waveform. As can be seen, after the resampling process, the shape of the waveform is truly identical to the transmission spectrum of the two cascaded FSLs that shown in Fig. 6(c). Fast Fourier transform (FFT) is then performed to the resampled waveform and the electrical spectrum is acquired. A digital low-pass filter with a rectangular function is used to filter out the high-frequency component of the resampled waveform. Then, inverse fast Fourier transform (IFFT) is performed to the filtered electrical spectrum and the envelope of the time domain microwave signal is acquired. The red curve in Fig. 6(b) shows the envelope of the microwave waveform. As the temperature applied to the sensing loop is changed, the envelope of the microwave signal will move accordingly. By measuring the time shift of a dip in the extracted envelope, the sensing information can be precisely demodulated.

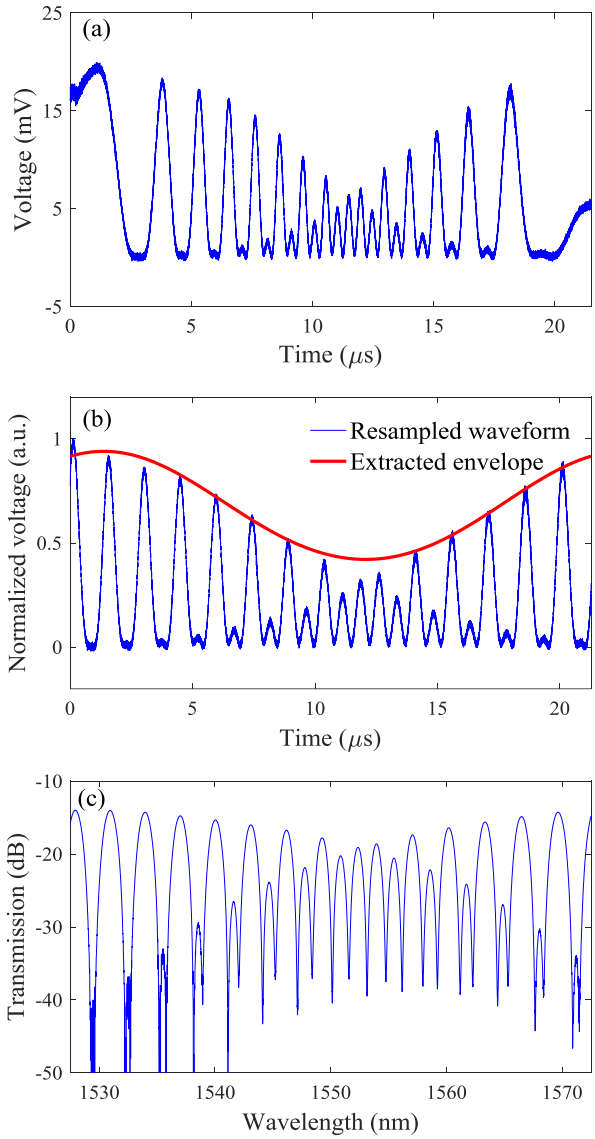

Fig. 6. Temporal microwave waveform sampled by a real-time oscilloscope after spectrally shaped by the two cascaded FSLs. (a) A negatively chirped optical pulse after spectrally shaped by the two cascaded FSLs. (b) Blue: the resampled signal; Red: the extracted envelope. (c) The measured transmission spectrum of the two cascaded FSLs that identical to the resampled waveform shown in (b).

To evaluate the sensing performance of the proposed fiber sensor, we increase the temperature which is applied to the first FSL and measure the time shift of the dip in the envelope. Fig. 7(a) shows the envelope changes as the temperature applied to the sensing loop is increased from 25.8 to 26.3 °C. As can be seen, when the temperature applied to the sensing loop is increased, the extracted envelope is shifted to a smaller time location accordingly. The time shifts of the dip in the extracted envelope are measured and the sensing information is demodulated. The blue curve in Fig. 7(b) shows the normalized time shift of the dip in the extracted envelope versus the temperature change. As can be seen, the dip in the extracted envelope is shifted from 5.8 to 0 μs with a good linearity when the temperature is increased from 25.8 to 26.3 °C. The temperature sensitivity of the proposed fiber sensor is calculated to be 12 μs/°C. The red curve shows the normalized wavelength shift of a dip of the single Sagnac loop versus the temperature change. The temperature sensitivity of the single Sagnac loop is calculated to be 1.8 nm/°C in the optical domain which equals to 0.95 μs/°C in the time domain. Both the single-loop wavelength shift and the extracted envelope time shift have good linear relation with the temperature, but with the R-square of the extracted envelope sensing curve ($R^2 = 0.9914$) is slightly lower than that of the single loop sensing curve ($R^2 = 0.9947$), which is caused by the waveform distortion and can be neglected. On the other hand, the sensitivity enhanced factor of the two cascaded Sagnac loops is calculated to be 12.6 which is close to the theoretically calculated enhanced factor according to (6). We attribute that this discrepancy is mainly caused by

Authorized licensed use limited to: Jianping Yao. Downloaded on December 16,2021 at 03:23:19 UTC from IEEE Xplore. Restrictions apply.

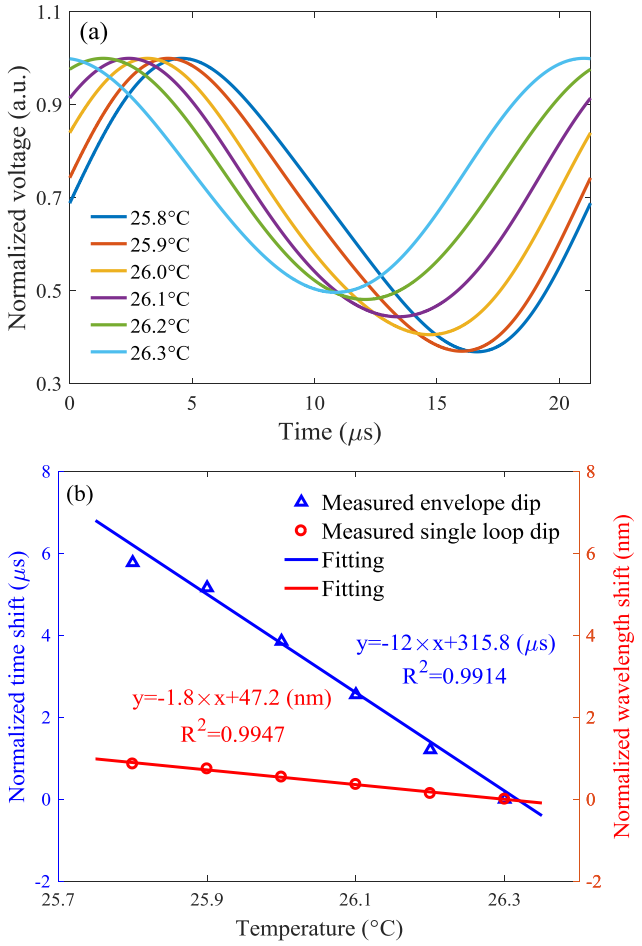

Fig. 7. Temperature change versus time shift of a dip in the envelope. (a) Extracted envelope changes as the temperature applied to the sensing loop is changed from 25.8 to 26.3 °C; (b) Blue: time shifts of the dip in the extracted envelope in the time domain; Red: wavelength shifts of a dip of the single Sagnac loop in the optical domain.

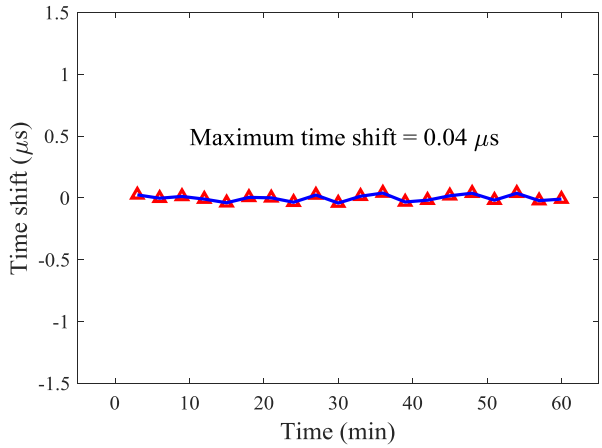

Fig. 8. Stability of the proposed temperature sensor.

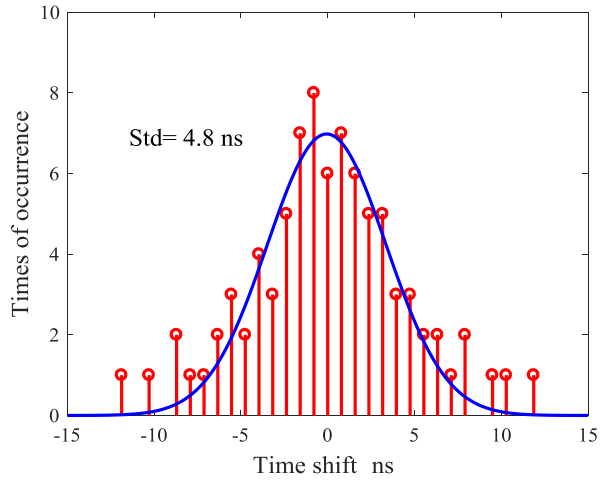

Fig. 9. Histograms of the time shift fluctuations of the dip in the extracted envelope when the temperature is 25.8 °C. The measurement number is 85.

the difference between the manufacturer provided birefringence coefficient and the actual birefringence coefficient, and the slight discrepancy of the length of each PMF. Considering that the real-time oscilloscope has a sampling rate of 6.25 GS/s, the temperature resolution is calculated to be 1.33×10^{-5} °C and due to the use of a high repetition rate FDML laser source, the sensing speed of the proposed system is as high as 23.497 kHz.

To extend the temperature measurement range of the proposed fiber-optic sensor, one of the solutions is to enlarge the wavelength scanning bandwidth of the FDML laser source which can be achieved by increasing the peak-to-peak voltage that applied to the tunable filter inside the laser cavity. A maximum scanning bandwidth of 80 nm can be obtained in our experiment. On the other hand, since there is a trade-off between the enhanced temperature sensitivity (a larger FSR of the envelope means a higher sensitivity) and the measurement range, the measurement range can be extended by sacrificing partially the sensitivity to reduce the FSR of the envelope.

The stability of the proposed temperature sensor is then evaluated. The sensing loop is placed in the temperature controller with a temperature of 25.8 °C within an hour and the time shift of the dip in the extracted envelope is measured. The time shift of the dip is shown in Fig. 8 and the maximum time shift of the dip is 0.04 μs, which is small indicating a good stability of the proposed sensor. The time shift of the dip can be attributed to the temperature fluctuations of the temperature controller and a tiny spectral shift of the FDML laser source.

On the other hand, the measurement accuracy of the proposed sensor is evaluated. In the experiment, 85 measurements are made by the real-time oscilloscope when the sensing loop is experiencing a temperature of 25.8 °C. The standard deviation of the time shift fluctuations of the dip in the extracted envelope is calculated to be 4.8 ns, which corresponds to a measurement accuracy of 4×10^{-4} °C. The deteriorated accuracy is mainly caused by the temperature fluctuations of the temperature controller, which can be reduced by using a temperature controller with smaller temperature fluctuations.

To realize a better sensing performance, the sensing speed can be improved by using a frequency swept laser source with a higher repetition rate and the temperature resolution can be

Authorized licensed use limited to: Jianping Yao. Downloaded on December 16,2021 at 03:23:19 UTC from IEEE Xplore. Restrictions apply.

improved by using a PD with a larger response bandwidth and a real-time oscilloscope with higher sampling rate, respectively.

IV. Conclusion

We proposed and experimentally demonstrated a high-speed and high-resolution fiber-optic temperature sensor based on two cascaded FSLs interrogated using microwave photonics method. Instead of monitoring the wavelength shift of the envelope of the two cascaded FSLs transmission spectrum in the optical domain by using an OSA with a low wavelength resolution and a slow scanning speed, we converted the transmission spectrum to the time domain based on SS-WTT mapping. A temporal microwave signal was obtained at the output of a PD. A real-time oscilloscope was used to sample the temporal microwave waveform which was processed by a DSP to extract the envelope of the temporal microwave waveform. By detecting a dip in the envelope, the wavelength shift due to temperature change was measured. Due to the high-speed and high-resolution of a real-time oscilloscope and a DSP used in the proposed sensing system, the sensing speed and resolution were greatly enhanced as compared with a conventional interrogation approach using an OSA. An experiment was implemented. The experimental results showed that the proposed fiber sensor was able to provide a temperature resolution of 1.33×10^{-5} °C with a sensing speed was as high as 23.497 kHz.

References

[1] Z. Zhu, L. Liu, Z. Liu, Y. Zhang, and Y. Zhang, "Surface-plasmon-resonance-based optical-fiber temperature sensor with high sensitivity and high figure of merit," *Opt. Lett.*, vol. 42, no. 15, pp. 2948–2951, Aug. 2017.

[2] Y. Cao *et al.*, "High-resolution and temperature-compensational HER2 antigen detection based on microwave photonic interrogation," *Sensor Actuators B, Chem*, vol. 245, pp. 583–589, Jun. 2017.

[3] T. L. Lowder, K. H. Smith, B. L. Ipson, A. R. Hawkins, R. H. Selfridge, and S. M. Schultz, "High-temperature sensing using surface relief fiber bragg gratings," *IEEE Photon. Technol. Lett.*, vol. 17, no. 9, pp. 1926–1928, Sep. 2005.

[4] V. Bhatia and A. M. Vengsarkar, "Optical fiber long-period grating sensors," *Opt. Lett.*, vol. 21, no. 9, pp. 692–694, May 1996.

[5] E. Chehura, S. W. James, and R. P. Tatam, "Temperature and strain discrimination using a single tilted fibre bragg grating," *Opt. Commun.*, vol. 275, no. 2, pp. 344–347, Jul. 2007.

[6] Y. Wang, M. Yang, D. N. Wang, and C. R. Liao, "Selectively infiltrated photonic crystal fiber with ultrahigh temperature sensitivity," *IEEE Photon. Technol. Lett.*, vol. 23, no. 20, pp. 1520–1522, Oct. 2011.

[7] W. Qian *et al.*, "High-sensitivity temperature sensor based on an alcohol-filled photonic crystal fiber loop mirror," *Opt. Lett.*, vol. 36, no. 9, pp. 1548–1550, May 2011.

[8] Y. Xue *et al.*, "Ultrasensitive temperature sensor based on an isopropanol-sealed optical microfiber taper," *Opt. Lett.*, vol. 38, no. 8, pp. 1209–1211, Apr. 2013.

[9] L. Shao *et al.*, "Sensitivity-enhanced temperature sensor with cascaded fiber optic sagnac interferometers based on Vernier-effect," *Opt. Commun.*, vol. 336, pp. 73–76, Feb. 2015.

[10] M. Quan, J. Tian, and Y. Yao, "Ultra-high sensitivity fabry–perot interferometer gas refractive index fiber sensor based on photonic crystal fiber and vernier effect," *Opt. Lett.*, vol. 40, no. 21, pp. 4891–4894, Nov. 2015.

[11] M. L. Notte and V. M. N. Passaro, "Ultra high sensitivity chemical photonic sensing by Mach-Zehnder interferometer enhanced Vernier-effect," *Sensor Actuators B, Chem*, vol. 176, pp. 994–1007, Jan. 2013.

[12] P. Zhang *et al.*, "Simplified hollow-core fiber-based Fabry–Perot interferometer with modified vernier effect for highly sensitive high-temperature measurement," *IEEE Photon. J*, vol. 7, no. 1, pp. 1–10, Feb. 2015.

[13] J. Yao, "Microwave photonics," *J. Lightw. Technol.*, vol. 27, no. 3, pp. 314–335, Feb. 2009.

[14] J. Capmany and D. Novak, "Microwave photonics combines two worlds," *Nature Photon.*, vol. 1, pp. 319–330, Jun. 2007.

[15] W. Liu, M. Li, C. Wang, and J. Yao, "Real-time interrogation of a linearly chirped fiber bragg grating sensor based on chirped pulse compression with improved resolution and signal-to-noise ratio," *J. Lightw. Technol.*, vol. 29, no. 9, pp. 1239–1247, May 2011.

[16] H. Deng, W. Zhang, and J. Yao, "High-speed and high-resolution interrogation of a silicon photonic microdisk sensor based on microwave photonic filtering," *J. Lightw. Technol.*, vol. 36, no. 19, pp. 4243–4249, Oct. 2018.

[17] R. Huber, M. Wojtkowski, and J. G. Fujimoto, "Fourier domain mode locking (FDML) a new laser operating regime and applications for optical coherence tomography," *Opt. Express*, vol. 14, no. 8, pp. 3225–3237, Apr. 2006.

[18] J. Yao, "Photonic generation of microwave arbitrary waveforms," *Opt. Commun.*, vol. 284, no. 15, pp. 3723–3736, Jul. 2011.

[19] G. Wang *et al.*, "High-speed and high-resolution microwave photonic interrogation of a fiber-optic refractometer with plasmonic spectral comb," *J. Lightw. Technol.*, vol. 38, no. 7, pp. 2073–2080, Apr. 2020.

[20] H. Deng, P. Lu, S. J. Mihailov, and J. Yao, "High-speed and high-resolution interrogation of a strain and temperature random grating sensor," *J. Lightw. Technol.*, vol. 36, no. 23, pp. 5587–5592, Dec. 2018.

Guangying Wang received the B.Eng. degree in optoelectronic information science and engineering from the Guangdong University of Technology, Guangzhou, China, in 2017. He is currently working toward the Ph.D. degree in optical engineering with the Institute of Photonics Technology, Jinan University, Guangzhou. His current research interests include microwave photonics sensing and signal processing.

Baoliang Liao received the B.Eng. degree in optoelectronic information science and engineering from Nanchang Hangkong University, Nanchang, China, in 2019. He is currently working toward the master's degree in optical engineering with the Institute of Photonics Technology, Jinan University, Guangzhou, China.

Yuan Cao received the B.S. degree from the Dalian University of Technology, Dalian, China, in 2011, and the Ph.D. degree from Jinan University, Guangzhou, China, in 2016. He is currently a Lecturer with the Institute of Photonics Technology, Jinan University. His research interests include microwave photonics signal processing & applications and optical biosensors.

Xinhuan Feng received the B.Sc. degree from Physics Department, Nankai University, Tianjin, China, in 1995, and the M.Sc. and Ph.D. degrees from the Institute of Modern Optics, Nankai University, in 1998 and 2005, respectively. From 2005 to 2008, she was a Postdoctoral Fellow with Photonics Research Centre, The Hong Kong Polytechnic University, Hong Kong. Since March 2009, she has been a Professor with the Institute of Photonics Technology, Jinan University, Guangzhou, China. Her research interests include various fiber active and passive devices and their applications, and microwave photonic signal processing.

Authorized licensed use limited to: Jianping Yao. Downloaded on December 16,2021 at 03:23:19 UTC from IEEE Xplore. Restrictions apply.

Bai Ou Guan received the B.Sc. degree in applied physics from Sichuan University, Chengdu, China, in 1994, and the M.Sc. and Ph.D. degrees in optics from Nankai University, Tianjin, China, in 1997 and 2000, respectively. From 2000 to 2005, he was at the Department of Electrical Engineering, The Hong Kong Polytechnic University, Hong Kong, first as a Research Associate, then as a Postdoctoral Research Fellow. From 2005 to 2009, he was at the School of Physics and Optoelectronic Engineering, Dalian University of Technology, Dalian, China, as a Full Professor. In 2009, he joined Jinan University, Guangzhou, China, where he founded the Institute of Photonics Technology. He has authored or coauthored more than 230 technical papers in peer-reviewed international journals and presented more than 30 invited talks at major international conferences. His current research interests include fiber optic devices and technologies, optical fiber sensors, biomedical photonic sensing and imaging, and microwave photonics. He received the Distinguished Young Scientist Grant from Natural Science Foundation of China (NSFC) in 2012. He is a Member of OSA, and was the General Chair/Co-Chair, Technical Program Committee or Subcommittee Chair/Co-Chair for more than 10 international conferences.

Jianping Yao received the Ph.D. degree in electrical engineering from the Université de Toulon et du Var, Toulon, France, in 1997. He is a Distinguished University Professor and University Research Chair with the School of Electrical Engineering and Computer Science, University of Ottawa, Ottawa, ON, Canada. From 1998 to 2001, he was at the School of Electrical and Electronic Engineering, Nanyang Technological University, Singapore, as an Assistant Professor. In 2001, he joined the School of Electrical Engineering and Computer Science, University of Ottawa as an Assistant Professor, where he was promoted to an Associate Professor in 2003, and to a Full Professor in 2006. He was appointed the University Research Chair in Microwave Photonics in 2007. In June 2016, he was conferred the title of Distinguished University Professor of the University of Ottawa. From 2007 to 2010 and from 2013 to 2016, he was the Director of the Ottawa-Carleton Institute for Electrical and Computer Engineering. He has authored or coauthored more than 620 research papers including more than 360 papers in peer-reviewed journals and more than 260 papers in conference proceedings. He is the Editor-in-Chief for the IEEE PHOTONICS TECHNOLOGY LETTERS, a Topical Editor for *Optics Letters*, an Associate Editor for *Science Bulletin*, a Steering Committee Member for the IEEE JOURNAL OF LIGHTWAVE TECHNOLOGY, and an Advisory Editorial Board Member for *Optics Communications*. He was a Guest Editor of a Focus Issue on Microwave Photonics in *Optics Express* in 2013, a Lead-Editor of a Feature Issue on Microwave Photonics in *Photonics Research* in 2014, and a Guest Editor of a Special Issue on Microwave Photonics in the IEEE JOURNAL OF LIGHTWAVE TECHNOLOGY in 2018. He is currently the Chair of the IEEE Photonics Ottawa Chapter and is the Technical Committee Chair of IEEE MTT-3 Microwave Photonics. He was a Member of the European Research Council Consolidator Grant Panel in 2016, the Qualitative Evaluation Panel in 2017, and a Member of the National Science Foundation Career Awards Panel in 2016. He was also a Chair of a number of international conferences, symposia, and workshops, including the Vice Technical Program Committee (TPC) Chair of the 2007 IEEE Topical Meeting on Microwave Photonics, TPC Co-Chair of the 2009 and 2010 Asia-Pacific Microwave Photonics Conference, TPC Chair of the High-Speed and Broadband Wireless Technologies Subcommittee of the IEEE Radio Wireless Symposium 2009–2012, TPC Chair of the Microwave Photonics Subcommittee of the IEEE Photonics Society Annual Meeting 2009, TPC Chair of the 2010 IEEE Topical Meeting on Microwave Photonics, General Co-Chair of the 2011 IEEE Topical Meeting on Microwave Photonics, TPC Co-Chair of the 2014 IEEE Topical Meetings on Microwave Photonics, and General Co-Chair of the 2015 and 2017 IEEE Topical Meeting on Microwave Photonics. He was also a Committee Member for a number of international conferences, such as IPC, OFC, BGPP, and MWP. He was the recipient of the 2005 International Creative Research Award of the University of Ottawa, the 2007 George S. Glinski Award for Excellence in Research, a Natural Sciences and Engineering Research Council of Canada Discovery Accelerator Supplements Award in 2008, an inaugural OSA Outstanding Reviewer Award in 2012, and the Award for Excellence in Research 2017–2018 of the University of Ottawa. He was one of the top ten reviewers of IEEE/OSA JOURNAL OF LIGHTWAVE TECHNOLOGY from 2015 to 2016. He was an IEEE MTT-S Distinguished Microwave Lecturer for 2013–2015. He is a registered Professional Engineer of Ontario. He is a Fellow of the Optical Society of America, the Canadian Academy of Engineering, and the Royal Society of Canada.

Authorized licensed use limited to: Jianping Yao. Downloaded on December 16,2021 at 03:23:19 UTC from IEEE Xplore. Restrictions apply.